Research

This article has been edited by the Royal Society of Chemistry, including the commissioning, peer review process and editorial aspects up to the point of acceptance.

Electronic supplementary material is available online at https://doi.org/10.6084/m9.figshare.c.6182406.

Macrolactonization of methyl 15-hydroxypentadecanoate to cyclopentadecanolide using KF-La/γ-Al$_2$O$_3$ catalyst

Haijun Cheng, Chang Yu, Hongyun Wang, Xiongmin Liu, Li Ma and Fang Lai

School of Chemistry and Chemical Engineering, Guangxi University, Nanning Guangxi 530004, People's Republic of China

HC, 0000-0002-4542-614X; CY, 0000-0002-1198-9198; XL, 0000-0003-1044-4548; FL, 0000-0001-6710-9578

It has been a challenge to synthesize macrolide musk in excellent yields with high purity. KF-La/γ-Al$_2$O$_3$ catalyst was prepared from a highly basic mesoporous framework using a mild method. The prepared KF-La/γ-Al$_2$O$_3$ catalyst was employed for the synthesis of cyclopentadecanolide from methyl 15-hydroxypentadecanoate. The morphology and structure of prepared catalysts were characterized using XRD, TG-DTG, SEM, EDX, TEM, BET and CO$_2$-TPD. The results revealed that the K$_3$AlF$_6$ and LaOF are produced on the surface of KF-La/γ-Al$_2$O$_3$, and LaO can promote the dispersion of KF on the surface of Al$_2$O$_3$. Catalysts pore size main distribution ranges between 10 and 30 nm, the maximum CO$_2$ desorption temperature is 715°C when the La loading is 25%. Because F$^-$ ion has a higher electronegativity than O^{2-} ion, the KF-promoted metal oxide (Al$_2$O$_3$ or/and La$_2$O$_3$) contained more strong basic sites, compared with that of the corresponding metal oxide. The yield of cyclopentadecanolide obtained at 0.5 g KF-25La/γ-Al$_2$O$_3$ catalyst and a reaction temperature of 190°C for 7 h were 58.50%, and the content after reactive distillation is 98.8%. The KF-La/γ-Al$_2$O$_3$ catalyst has a larger pore size and basic strength, which is more conducive to the macrolactonization of long-chain hydroxy ester.

1. Introduction

Macrolactones are lactones containing more than eight atoms in the lactone ring. The structural motifs of macrolactone are widely observed in natural products, drug molecules and bioactive molecules [1,2]. Macrolactones are commonly used to produce biological pheromones, drugs [3–6], pesticides [7],

antimicrobial agents and spices [8]. Macrolactones containing 15–17 carbon atoms have attracted significant attention in the cosmetic industry as a substitute for natural musks because of their unique fragrance. This could be attributed to the fact that they do not display the cancerogenic and bioaccumulation toxic properties [9–11] associated with nitro-musks and polycyclic-musks. In addition, the cost of synthesizing macrolactones is significantly lower than that of extracting natural musk. Consequently, in the past decades, macrolactonization reactions have attracted increased attention among researchers.

Macrolides can be artificially synthesized using chemical methods [12]. It is well known that long-chain hydroxy fatty acids do not readily form macrolides compounds via macrolactonization owing to the binding of reactive molecules, which leads to the formation of dimers or oligomers. Therefore, these methods require the use of catalyst to increase the macrolides yields [13]. The chemical synthesis of macrolactone is a cost-effective procedure [14–16]. Conventional methods for macrolide synthesis typically include: a direct macrolactonization of the corresponding seco-acid [14,15,17–20], ring-closing metathesis [21,22], cross-coupling reactions [23–26], macrolactonization of alkenyl acid, macrocyclic olenation reactions [27] and catalytic carbonylative macrolactonization [28,29]. Additionally, catalytic C–H macrolactonization [18,30], enantioselective Rh-catalysed redox-neutral allene-acid macrocyclization [31] and NHC-catalysed oxidative macrolactonization [32] as an unconventional method have also been explored. Currently, direct macrolactonization of the corresponding seco-acid still remains the most prevalent method. In 1985, Boden & Keck used ω-hydroxy acids of various chain lengths as the raw material 4-dimethylaminopyridine (DMAP) as the catalyst to react in dicyclohexylcarbodiimide (DCC) solution for 16 h to synthesize the corresponding macrolide compound, and the product was isolated and purified, which affords a 95% isolated yield of hexadecanolide [16]. Mukaiyama *et al.* prepared medium-sized lactones on treating monomeric cyclic silyl siloxycarboxylates, prepared *in situ* from ω-hydroxycarboxylic acids and 1,2-bisdimethylsilylbenzeneusing $RhCl(PPh_3)_3$ catalyst, with an active catalyst of dimethylsilylbis (trifluoromethanesulfonate) [33]. In this experiment, 10 ml of benzene was added as a solvent, and the amount of ω-hydroxy acids added was 0.2 mmol. After 18 h of reaction, column chromatography on silica to afford lactone, the highest yield was 87%. Shiina *et al.* [34] described an efficient method for the synthesis of various esters, involving the intermediary formation of a mixed anhydride with benzoic acid anhydrides in the presence of catalytic amounts of Lewis acids. $TiCl_4$, toluene and chlorotrimethylsilane were used as active reagents, and dichloromethane was used as solvent. Finally, the crude product was purified by thin layer chromatography and the highest yield of macrolide was 83%. Ookoshi & Onanka reported the macrolactonization of ω-hydroxyalkanoic acid is catalysed by dealuminated HY zeolite in a concentrated toluene solution [35]. The highest yield of macrolide was 51% after 24 h of reaction. De Léséleuc & Collins used $Hf(OTf)_4$ to catalyse the direct macrolactonization of seco-acid (5 mmol l^{-1}) in the presence of toluene as a solvent, and the highest macrolide yield of 87% was obtained at 100°C for 24 h [36]. However, there are several inherent limitations associated with traditional seco-acid methods. For example, a stoichiometric amount of activating reagents are required for the activation of either the acid or the hydroxyl group [3]. The reaction time is excessively long, whereas the intermolecular synthetic processes always occur along with competitive reactions, leading to the undesired polymer as by-products [37]. In addition, to minimize intermolecular dimerization, highly diluted conditions or slow addition protocols are required [38,39] and selectivity in the closed-loop reaction step is poor [40], which has the low synthetic efficiency and economy. The reagents used in the experiment are highly toxic, especially the liquid catalysts which are prone to corrode the equipment, make post-treatment difficult and pose a threat to the environment.

Although Ookoshi & Onanka [35] and Lai *et al.* [37] used solid acid as catalyst, a large amount of organic solvent was added during the reaction, and the product needed to be purified. To the best of our knowledge, the development of heterogeneous solid base catalysts has attracted significant attention in recent years [41,42]. For example, solid base catalysts have been widely employed in transesterification owing to its eco-friendliness and remarkable activity [43–47]. We can roughly divide solid base catalysts into two types. One is an unsupported solid base, which includes alkaline earth metal oxides, rare earth oxides and composite oxides. The other is supported solid bases, namely alkali metal oxides and hydroxides supported on various porous materials, etc. [48].

The catalytic activity of a solid base catalyst is determined by its solid structure and surface characteristics, particularly, its basicity and specific surface area. Usually, in order to enhance base strength, alkaline-earth oxide, rare-earth oxide and their mixed oxides frequently modified with potassium compounds, including KF, K_2CO_3, KOH and K_2O [49–52]. KF-loaded metal oxides exhibit high catalytic activity to macrolactonization [53]. La_2O_3 is widely used as a basic carrier or catalytic promoter owing to its low polarizing power [54]. Although KF-supported La_2O_3 exhibits strong

basicity, it has the disadvantages of high calcination temperature, small specific surface area and low selectivity. To obtain a solid base catalyst with a large specific surface area [55,56], Liu *et al.* [57] used La_2O_3 as a protection medium for SBA-15 support. The combination of KF and La_2O_3 facilitated the generation of super basic sites to obtain a solid base catalyst with an average pore diameter of approximately 5 nm. However, the high cost and relatively small average pore size of SBA-15 support limit its application in catalysing macromolecular species reactions [35]. Therefore, the development of supported solid superbases is beneficial to catalyse macrolactonization reactions.

Among various supports, γ-Al_2O_3 has attracted significant attention among researchers as a mesoporous material [58,59] owing to its large specific surface area, favourable dispersibility, thermostability [60] and high catalytic performance [61,62]. The addition of La is known to stabilize alumina for high temperature applications and Lanthanum acts as a promoter in combination with Al_2O_3 to render the solid strongly basic [63,64]. Considering that methyl 15-hydroxypentadecanoate is a long-chain macromolecule containing 16 carbon atoms. In this study, a modified wetness impregnation method was used to sequentially load La_2O_3 and KF on the surface of γ-Al_2O_3 at mild calcination temperature, which avoided the decomposition of nitrate anion at high temperature brought by potassium. The synthesized strong basic KF-La/γ-Al_2O_3 solid catalyst exhibited a large specific surface area and pore size [65,66]. The structure, surface area, basicity and thermal stability of the prepared KF-La/γ-Al_2O_3 mesoporous solid base catalyst were characterized using XRD, TG-DTG, SEM, EDX, TEM, BET and CO_2-TPD. Methyl 15-hydroxypentadecanoate ester was used as the raw material for the macrolactonization. Under the presence of the synthesized KF-La/γ-Al_2O_3 solid base, a high value-added musk containing cyclopentadecanolide was obtained. The formation of the macrolide does not require more than stoichiometric amounts of reagents to activate the carboxylate or the alcohol. In this study, we discussed the formation process of the strong basic sites in the KF-La/γ-Al_2O_3 catalyst, and researched the influence of the structure and morphology of the catalyst and the macrolactonization of long-chain hydroxy ester and optimized the reaction conditions.

2. Material and methods

2.1. Chemicals

Malania Oleifera Chum oil was obtained from Yandong Township Bama County Guangxi province in China. Diethyl ether and sulfuric acid were purchased from Chengdu Kelong Chemical Co., Ltd (Chengdu, China). Methanol and ethanol were purchased from Xilong Scientific Co., Ltd (Guangdong, China). n-hexane and glycerine were purchased from Guangdong Guanghua Sci-Tech Co., Ltd (Guangdong, China). Cyclopentadecanolide (greater than 98%) was purchased from Sigma-Aldrich Co., γ-Al_2O_3 (purity greater than 99.9%), lanthanum nitrate hexahydrate and 2-amino-2-methyl-1-propanol were purchased from Shanghai Aladdin Biochemical Technology Co., Ltd (Shanghai, China). Potassium fluoride was purchased from Shanghai Macklin Biochemical Co., Ltd (Shanghai, China). All reagents are analytical grade.

2.2. Catalyst preparation

KF-La/γ-Al_2O_3 was synthesized according to the reported method [67] as follows: La_2O_3 was introduced to γ-Al_2O_3 using the incipient wetness impregnation method. Typically, γ-Al_2O_3 was roasted in a muffle furnace at 550°C for 3 h. Simultaneously, 0.78 g of $La(NO_3)_3 \cdot 6H_2O$ was dissolved in 40 ml ethanol, after which 1.0 g of γ-Al_2O_3 was added into the mixture. Subsequently, the resulting mixture was stirred at 40°C for 24 h, after which the mixture was heated and stirred in an oil bath at 60°C until the solvent evaporated. Thereafter, the obtained solid was dried at 60°C overnight. Lastly, the precursor was calcined in a muffle furnace at 550°C for 4 h to convert $La(NO_3)_3$ to La_2O_3. The resulting γ-Al_2O_3-supported La oxides were denoted as $(\omega)La/\gamma$-Al_2O_3, where ω is the La/Al_2O_3 mass ratio.

KF was introduced to the surface of the as-synthesized $(\omega)La/\gamma$-Al_2O_3 using the wetness impregnation method. First, 0.2 g of KF was dissolved in 40 ml of absolute methanol, after which $(\omega)La/\gamma$-Al_2O_3 was added to the mixture. Subsequently, the mixture was stirred at room temperature until the solvent evaporated, after which the precipitate was dried for 24 h under vacuum at 60°C. The obtained catalyst precursor was calcined in a muffle furnace at 350°C for 4 h, during which KF was activated, leading to the formation of KF-$(\omega)La/\gamma$-Al_2O_3. KF/γ-Al_2O_3 and La/γ-Al_2O_3 were also synthesized using the aforementioned methods.

2.3. Synthesis of methyl 15-hydroxypentadecanoate

Methyl 15-hydroxypentadecanoate was synthesized using the following method. First, *Malania Oleifera Chum* oil was subjected to saponification, acidification, and solvent crystallization to obtain 15-tetracosenoic acid. Subsequently, 30.0 g of 15-tetracosenoic acid was added to a solution composed of 40 ml of ethanol and 160 ml of n-hexane. The mixed solution was placed in a thermostatic water bath at 0°C, after which the mixture was exposed to ozone generated using a laboratory-scale corona discharge generator continuously bubbling into the reactor. A change in the colour of a wet starch potassium iodide test paper to blue was used to indicate the end of the ozonation reaction. The obtained ozonide intermediate was added into a beaker, after which potassium borohydride solution was slowly added into the beaker and continuously stirred for 3 h. Lastly, 6 mol l^{-1} of hydrochloric acid was added to the solution until the pH value of the solution was 2, after which the solution was filtrated, washed to neutrality with deionized water and dried under vacuum at 70°C to obtain 15-hydroxypentadecanoic acid.

The prepared 15-hydroxypentadecanoic acid was purified using 2-amino-2-methyl-1-propanol to obtain an amine compound. Subsequently, the compound was subjected to methyl esterification reaction by dissolving 15 g of 15-hydroxypentadecanoic acid in 300 ml of methanol, after which 2 ml of concentrated sulfuric acid was added into the mixture. The obtained mixed solution was reacted in a thermostatic oil bath at 90°C for 4 h in a reflux device. After the reaction, the mixed solution was extracted using ether, and then washed with deionized water. The solvent in the upper layer of the solution separated from the mixed solution was removed using a rotary evaporator under vacuum condition at 70°C. Lastly, methyl 15-hydroxypentadecanoate with an average content of 90% was obtained.

2.4. Catalysts characterization

The XRD patterns of the samples were recorded using a Rigaku Ultima IV diffractometer with monochromatic Cu K$_\alpha$ radiation (λ = 1.5418 nm) in the 2θ ranges of 10–80°.

TGA analysis was performed using a TA Instruments Q500 Thermogravimetric Analyzer. To prepare the TGA sample, 10.0 mg of the catalyst was placed in a sample pan, after which the catalyst was heated from 30 to 750°C at a rate of 10°C min^{-1} under nitrogen atmosphere. The TGA analysis was performed under nitrogen atmosphere, and the total flow rate was maintained at 35.0 ml min^{-1}.

The microscopic morphology and surface structure of the catalysts were characterized using TEM (FEI Talos F200 s, USA), and the chemical composition of the catalysts was examined using SEM-EDX (Hitachi SU-5000, Japan).

The specific surface area, pore-volume and pore size of the catalysts were measured using a NOVA 2200e gas sorption analyser (Quantachrome Company, Boynton Beach, FL, USA) via N$_2$-physisorption adsorption and desorption at −196°C. Before testing, the catalyst was degassed under nitrogen atmosphere at 120°C for 2 h. The specific surface areas of the catalysts were calculated using the Brunauer–Emmett–Teller (BET) method, and the pore volume and diameter were calculated using the Barrett–Joyner–Halenda (BJH) model.

CO$_2$-TPD was used to measure the total basicity and basic strength distribution of the catalyst using a FINESORB-3010 apparatus equipped with a thermal conductivity detector. To prepare the sample used for the analysis, 50.0 mg of the catalyst samples (40–60 mesh) were pretreated at 110°C under helium flow (99.999%) at a rate of 10 ml min^{-1} for 1 h, and the samples were saturated with pure CO$_2$ flow after cooling to room temperature. Subsequently, the pretreated samples were purged in helium atmosphere at room temperature until the baseline was sufficiently stable to remove physisorbed CO$_2$. Thereafter, the samples were heated from room temperature to 850°C at 10°C min^{-1} under helium flow.

2.5. Evaluation of catalytic performance

The as-synthesized methyl 15-hydroxypentadecanoate was used for the synthesis of cyclopentadecanolide. Typically, methyl 15-hydroxypentadecanoate (5 mmol), KF-La/γ-Al$_2$O$_3$ catalyst (0.5 g) and glycerine (15 ml) were mixed and stirred for 30 min at 120°C using an electric heater with magnetic stirring. Subsequently, the system was slowly heated to 190°C under 2 mbar pressure and maintained for 7 h. The produced cyclopentadecanolide was separated from the reaction system using the reaction–distillation method through an oil–water separator. The reaction–distillation reaction shifted the chemical equilibrium in favour of the formation of cyclopentadecanolide. The cyclopentadecanolide crystals floating on the surface of glycerol were collected.

2.6. Analysis of products

Methyl 15-hydroxypentadecanoate and cyclopentadecanolide were analysed using Ultra gas chromatography mass spectrometry (GC-MS, Shimadzu GCMS-QP2010). To calculate the yield of the target products, the products were detected using gas chromatography (Shimadzu GC-2010 Plus). The cyclopentadecanolide product yield was calculated as follows:

$$\text{yield}\ (\%) = \frac{m(\text{product})}{m(\text{theory})} \times 100\%$$

3. Results and discussion

3.1. Characterization of the catalyst

3.1.1. Structure of the catalyst

The XRD patterns of the γ-Al$_2$O$_3$, La/γ-Al$_2$O$_3$, KF/γ-Al$_2$O$_3$, KF-La/γ-Al$_2$O$_3$ and KF/La$_2$O$_3$ catalysts are shown in figure 1. Distinct characteristic peaks were observed in the XRD patterns of the pure γ-Al$_2$O$_3$ with significant intensity at $2\theta = 36.8$, 39.6, 46.5 and 67.2° (PDF# 49-0134).

However, no clear and sharp diffraction peaks associated with the supported metal crystallites were observed in the XRD pattern of the La/γ-Al$_2$O$_3$ samples. In addition, the intensity of the diffraction peak of γ-Al$_2$O$_3$ was significantly weakened. This suggests that the introduced La species were evenly dispersed on the γ-Al$_2$O$_3$ support as amorphous phases or nanocrystals. Characteristic peak of La$_2$(CO$_3$)$_3$ (PDF# 25-1400) were observed in the XRD pattern of La/γ-Al$_2$O$_3$ at $2\theta = 22.5$ and 29.5°, which could be attributed to the fact that La$_2$O$_3$ readily reacts with CO$_2$ in air to form La$_2$(CO$_3$)$_3$. Diffraction peaks were observed in the XRD pattern of the KF/γ-Al$_2$O$_3$ catalyst at $2\theta = 18.0$, 29.7, 42.8 and 62.0° (PDF# 03-0615), which could be attributed to the presence of K$_3$AlF$_6$ in the sample. In addition, the intensity of the γ-Al$_2$O$_3$ peak decreased, which could be attributed to the fact that the surface of γ-Al$_2$O$_3$ was covered with KF and K$_3$AlF$_6$. In addition to the diffraction peaks of K$_3$AlF$_6$ and Al$_2$O$_3$, new diffraction peaks were observed in the XRD pattern of KF-(ω)La/γ-Al$_2$O$_3$ at $2\theta = 26.7$, 30.5, 44.1 and 51.8°(PDF# 77-0204), which could be attributed to the presence of LaOF. Furthermore, only a small peak corresponding to K$_3$AlF$_6$ was observed in the XRD pattern of the KF-La/γ-Al$_2$O$_3$ catalyst at $2\theta = 29.7°$, and other characteristic peaks disappeared. This could be attributed to the fact that: (i) the uniform covering of La$_2$O$_3$ on the surface of γ-Al$_2$O$_3$ hindered the reaction between KF and γ-Al$_2$O$_3$; (ii) most of the KF reacted with La$_2$O$_3$ to form LaOF, thus diffraction peak of La$_2$(CO$_3$)$_3$ or La$_2$O$_2$CO$_3$ were not observed in the XRD pattern of the KF-La/γ-Al$_2$O$_3$ catalyst. This indicates that the introduction of KF improved the CO$_2$ resistance of the La/γ-Al$_2$O$_3$ catalyst and prevented the consumption of the basic site by acid gases, such as CO$_2$ [68]. In addition, peaks relating to KF were not observed, which could be attributed to the high dispersion of KF on the surface of the catalyst. These findings indicate that the γ-Al$_2$O$_3$ of the KF-(ω)La/γ-Al$_2$O$_3$ catalyst was sequentially covered with La$_2$O$_3$ and KF, and a new compound (i.e. LaOF) was formed on the outermost layer.

The XRD patterns of the KF-(ω)La/γ-Al$_2$O$_3$ (ω = 15, 20, 25, 30 and 35%, where ω is the La/Al$_2$O$_3$ mass ratio) catalysts with different La loading are shown in figure 2. The major diffraction peaks in the XRD patterns of the samples are the peaks of LaOF, K$_3$AlF$_6$ and Al$_2$O$_3$. In addition, the XRD results revealed that the intensity of the characteristic peaks of LaOF gradually increased with an increase in the La species loading in γ-Al$_2$O$_3$, whereas the strength of the characteristic peaks of K$_3$AlF$_6$ ($2\theta = 29.7$, 42.8, 62.0°) reduced. This indicates that an increase in the La loading content facilitated the formation of LaOF, as the La species hindered the reaction between KF and Al$_2$O$_3$. It can be concluded that both La$_2$O$_3$ and KF have been supported on γ-Al$_2$O$_3$, and LaOF metal salts are formed on the surface, which may have a direct impact on the catalytic macrolactonization.

3.1.2. TG-DTA results of the La/γ-Al$_2$O$_3$ before and after calcination

The TG and DTG curves of the as-prepared La/γ-Al$_2$O$_3$ before and after calcination are shown in figure 3. The first weight loss of the uncalcined La/γ-Al$_2$O$_3$ was observed between 30°C and 150°C, which could be attributed to the removal of the methanol solvent and water molecules. The second weight loss was observed between 330°C and 550°C, which could be attributed to the conversion of lanthanum nitrate to lanthanum oxide. In contrast, only one weight loss was observed in the DTG curves of the calcined
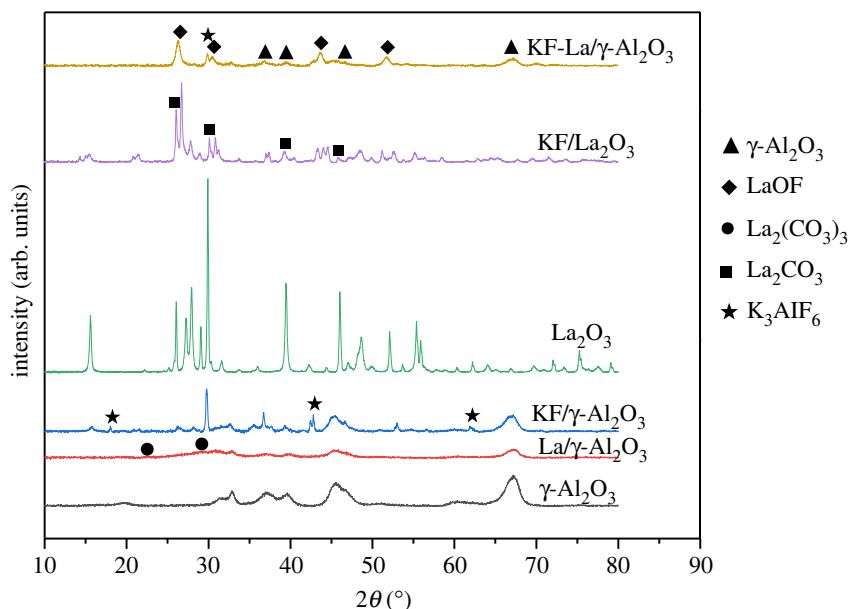
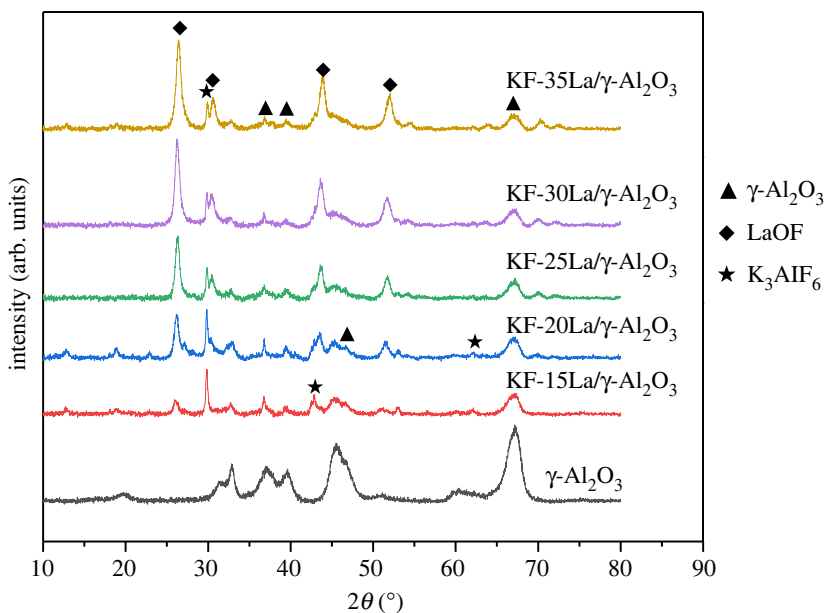**Figure 1.** X-ray diffraction patterns of the different synthesized catalysts.

Figure 2. X-ray diffraction patterns of the KF-La/γ-Al$_2$O$_3$ catalysts with different La loadings.

La/γ-Al$_2$O$_3$ catalyst at approximately 150°C, which could be attributed to the removal of water molecules. In addition, there was no significant weight loss after 230°C, indicating the complete conversion of the lanthanum nitrate on the surface of the La/γ-Al$_2$O$_3$ catalyst to lanthanum oxide. These results indicate that the optimum calcination temperature was 550°C.

During calcination, La-O species attached to Al–O species to form a dense layer on the surface of the γ-Al$_2$O$_3$ support [69]. Consequently, this enhanced the even dispersion of La species on the surface, as confirmed by the XRD results. The possible dispersion of La$_2$O$_3$ on Al$_2$O$_3$ is shown in figure 4.

3.1.3. Morphology and composition of the catalysts

The morphology of the KF-(ω)La/γ-Al$_2$O$_3$ catalysts with different La loadings was characterized using SEM, and the results are shown in figure 5. The SEM images revealed that γ-Al$_2$O$_3$ exhibited a non-spherical morphology and irregular particles with a size of 1–10 µm (figure 5a_1). In addition, the particles exhibited a rough surface (figure 5a_2). Furthermore, a comparison of figure 5b_1–f_1 and
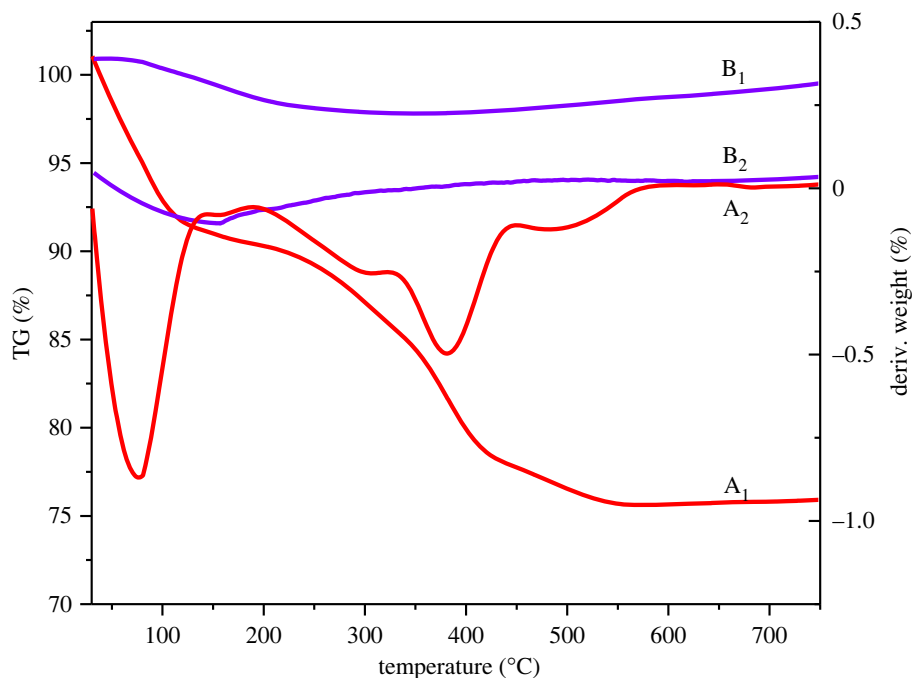
Figure 3. TG and DTG curves of the La/γ-Al$_2$O$_3$ before (A1 and A2) and after (B1 and B2) calcination.

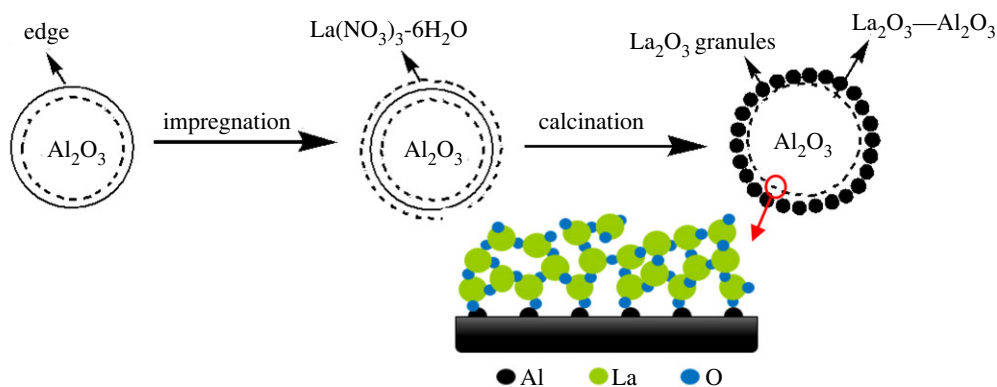**Figure 4.** Proposed formation process of La/γ-Al$_2$O$_3$.

figure 5b_1,c_1,e_1,f_1 reveals the presence of notable agglomeration on the surface of the particles, which is consistent with the high-magnification SEM image in figure 5b_2,c_2,e_2,f_2. As shown in figure 5b,c, agglomeration can be observed on the surface of the KF-15La/γ-Al$_2$O$_3$ and KF-20La/γ-Al$_2$O$_3$ catalysts, which could be attributed to the reaction between KF Al$_2$O$_3$. With an increase in the La loading to 35%, several agglomerated particles were observed on the surface of the KF-30La/γ-Al$_2$O$_3$ and KF-35La/γ-Al$_2$O$_3$ catalyst (figure 5e_1,f_1), thus giving the surface of the catalyst a smooth appearance (figure 5e_2,f_2). This could be attributed to the excessive accumulation of La$_2$O$_3$. However, there was no change in the particle size of the KF-25La/γ-Al$_2$O$_3$ catalyst as there was no agglomeration of particles, and the surface roughness was high (figure 5d_1,d_2). This may be related to the uniform coverage of KF and La$_2$O$_3$ on the surface of γ-Al$_2$O$_3$, which is consistent with the XRD and EDX results. At a La loading of 25%, the catalyst exhibited a relatively good morphology.

The elemental composition and distribution of the KF-La/γ-Al$_2$O$_3$ catalyst were further investigated using EDX analysis, and the results are shown in figure 6a,b. For the EDX analysis, an area on the catalyst surface was selected, and the mass percentage of each element was measured. The mass percentages of O, F, Al, K and La were 68.27, 6.34, 16.86, 4.68 and 3.85%, respectively. Different colours were used to represent different elements. Al and O had the highest concentration with a relatively concentrated distribution, which could be attributed to the fact that Al$_2$O$_3$ was used as the support. By contrast, the
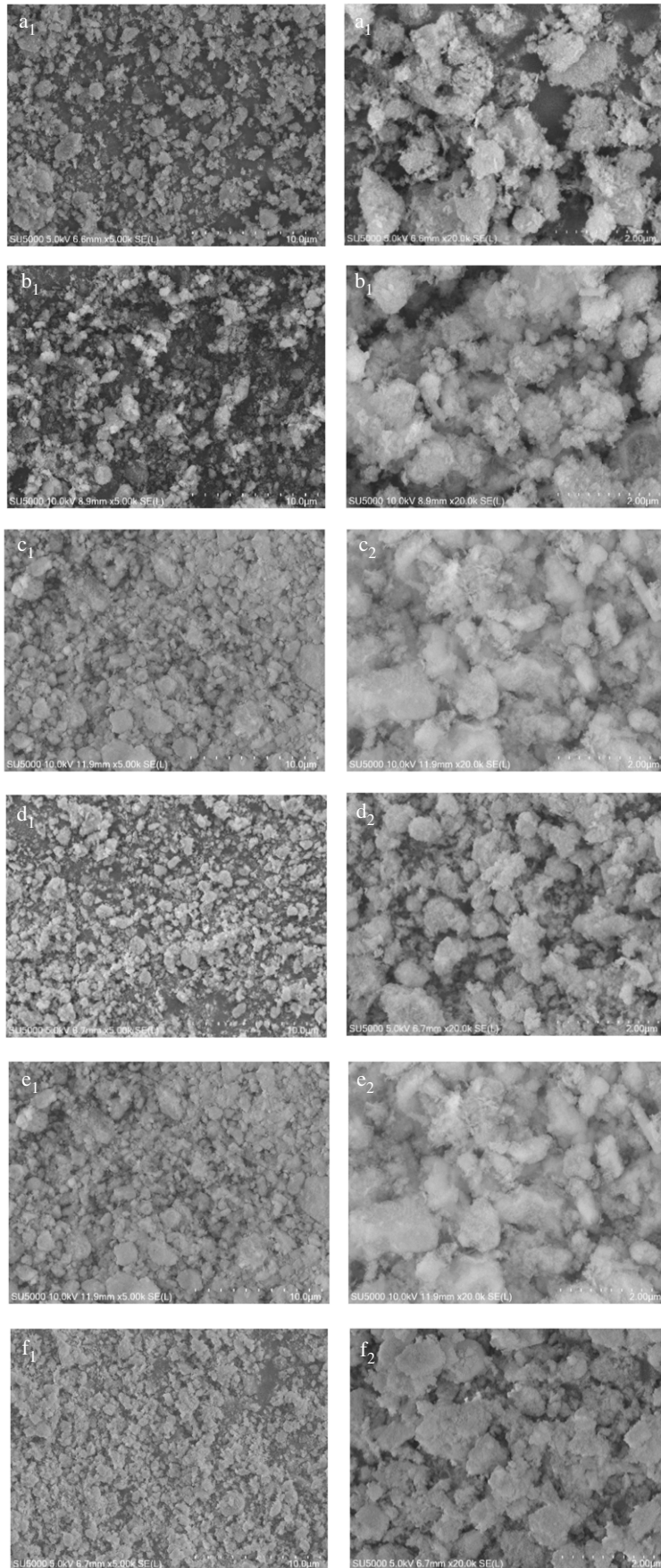
Figure 5. SEM images of (*a*) γ-Al$_2$O$_3$, (*b*) KF-15La/γ-Al$_2$O$_3$, (*c*) KF-20La/γ-Al$_2$O$_3$, (*d*) KF-25La/γ-Al$_2$O$_3$, (*e*) KF-30La/γ-Al$_2$O$_3$ and (*f*) KF-35La/γ-Al$_2$O$_3$.
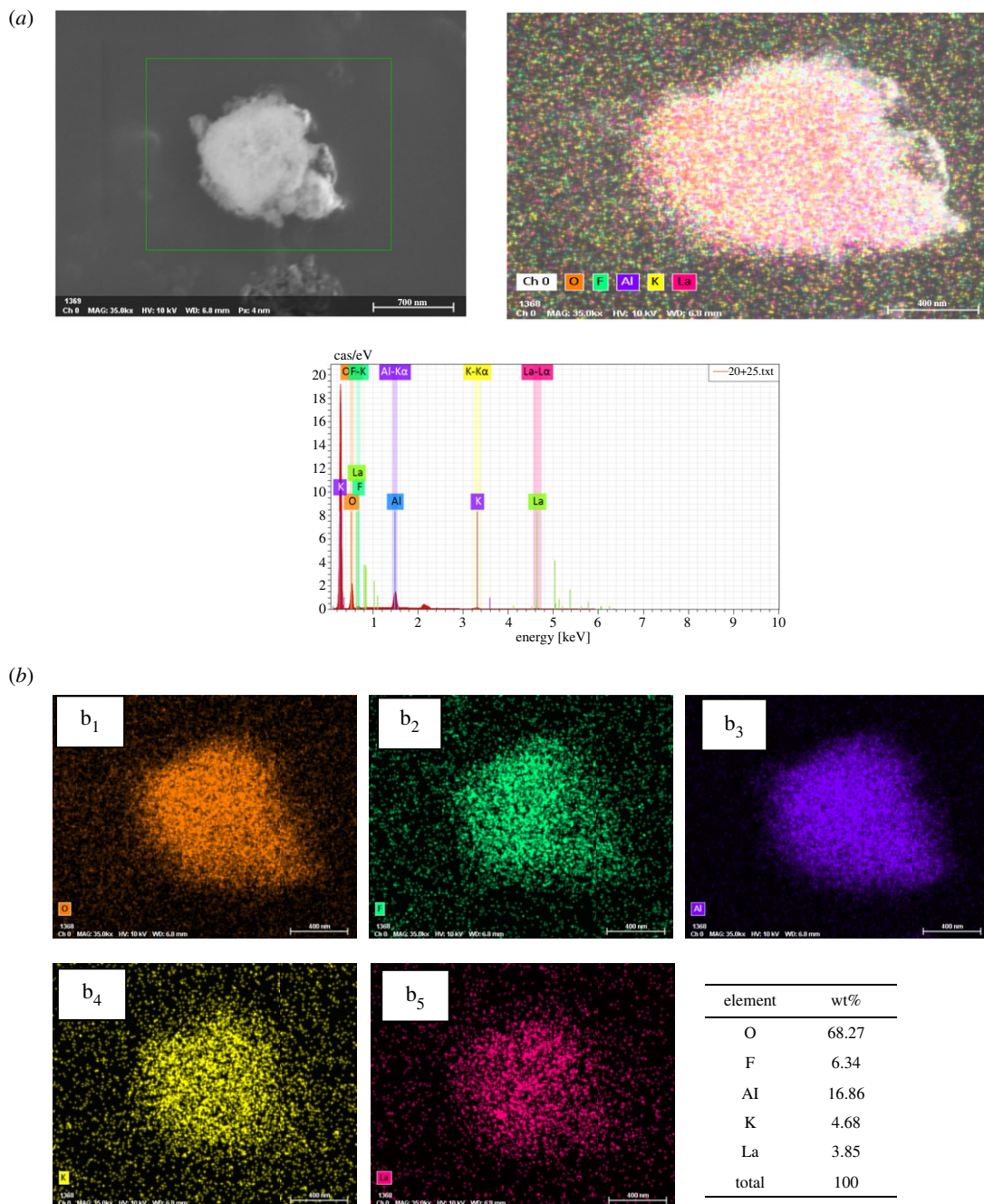
Figure 6. (*a*) SEM image for EDX mapping site and elemental spectrum for KF-La/γ-Al$_2$O$_3$ catalyst. (*b*). EDX elemental mapping of (b_1) O, (b_2) F, (b_3) Al, (b_4) K and (b_5) La of the KF-La/γ-Al$_2$O$_3$ catalyst.

element	wt%
O	68.27
F	6.34
Al	16.86
K	4.68
La	3.85
total	100

contents of other elements were relatively low, and they were uniformly distributed on the surface of the support, which is consistent with the XRD results.

The TEM images of the KF-La/γ-Al$_2$O$_3$ and γ-Al$_2$O$_3$ samples at different magnifications are shown in figure 7. The TEM images (figure 7a_1) revealed that there were substantial mesopores inside the γ-Al$_2$O$_3$ catalyst, which maintained a crack-shaped structure. This is consistent with the BET results. After the γ-Al$_2$O$_3$ was loaded with KF and La species, its channels became indistinct (figure 7b_1), which could be attributed to the uniform distribution of KF and La$_2$O$_3$ in the pores and the formation of LaOF on the surface of the catalyst. Figure 7a_2,a_3 shows the characteristic crystal planes and the corresponding lattice fringes of γ-Al$_2$O$_3$. Different crystal planes and lattice fringes (figure 7b_2) were observed in the TEM image of KF-La/γ-Al$_2$O$_3$. The lattice fringes can be roughly divided into three regions (figure 7b_3). According to the XRD results, these three regions corresponded to Al$_2$O$_3$, K$_3$AlF$_6$ and LaOF. Through the SEM, EDX and TEM analysis of KF-La/γ-Al$_2$O$_3$, we can clearly see the appearance of KF-La/γ-Al$_2$O$_3$, as well as the distribution of loaded KF and La$_2$O$_3$ on γ-Al$_2$O$_3$. This is advantageous for judging the proper load amount.
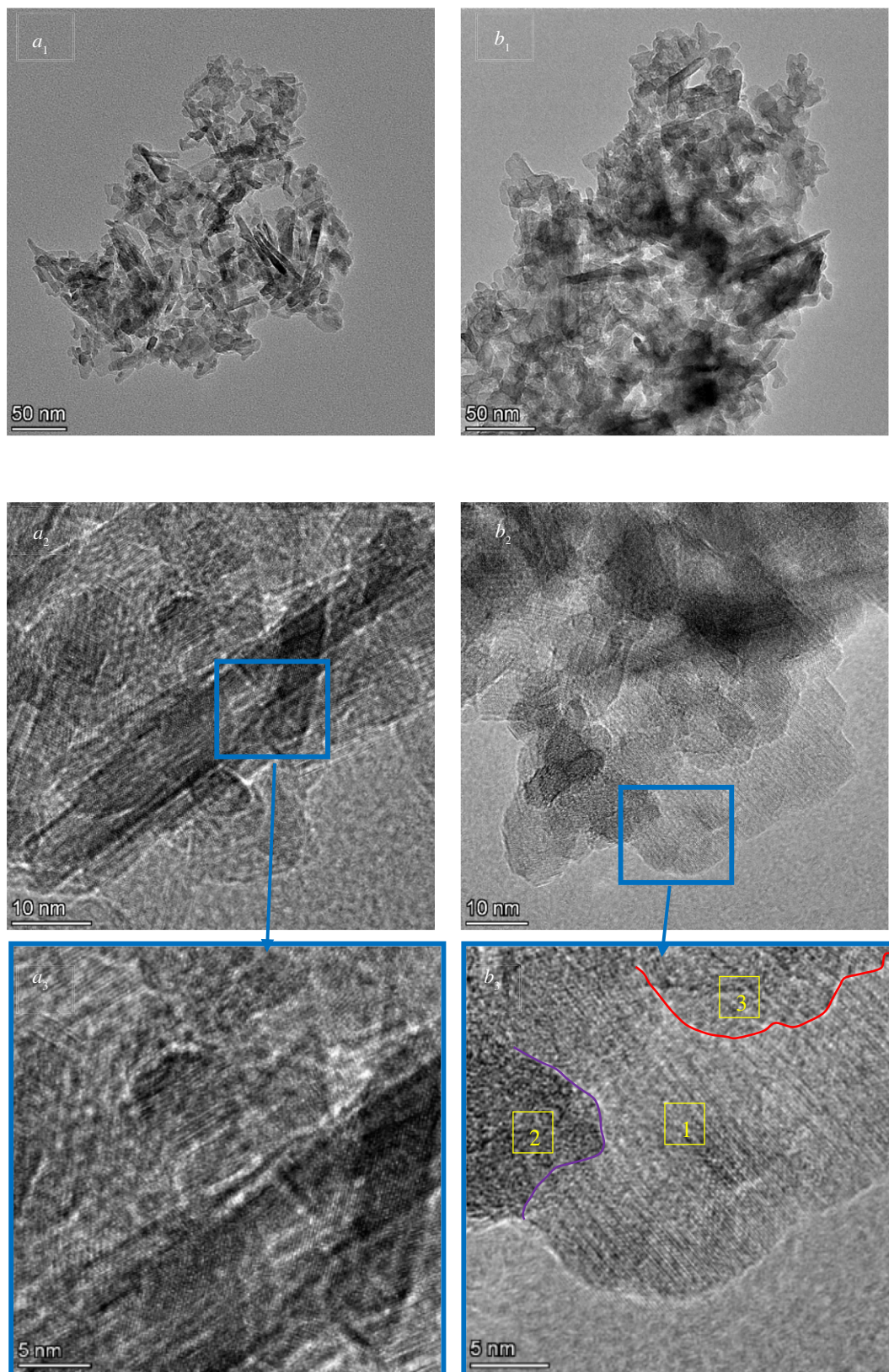
Figure 7. TEM images of the (*a*) γ-Al$_2$O$_3$ and (*b*) KF-La/γ-Al$_2$O$_3$ catalysts.

3.1.4. Surface area of the catalyst

The N$_2$ adsorption–desorption isotherms and pore size distribution of the catalysts with γ-Al$_2$O$_3$ as the carrier are shown in figure 8. Based on the adsorption isotherms classified by the International Union of Pure and Applied Chemistry (IUPAC), the results revealed that all the samples exhibited type IV
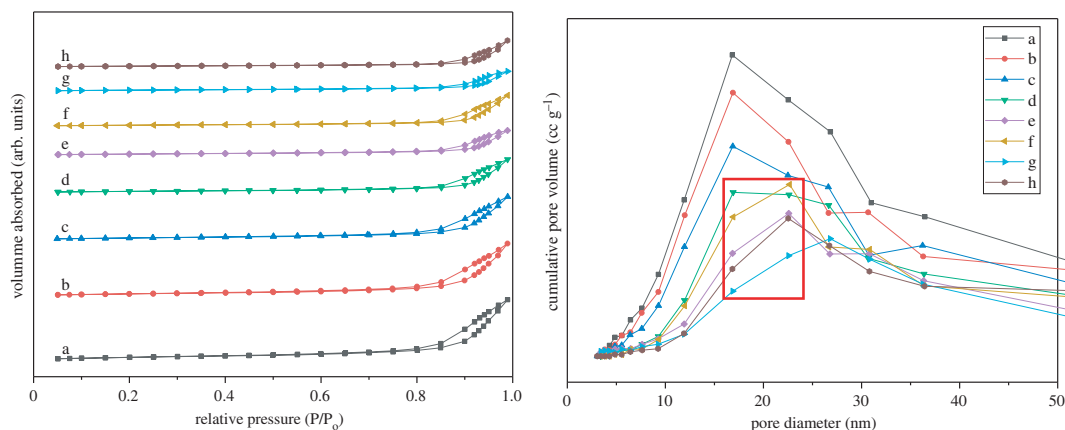
Figure 8. N_2 adsorption–desorption isotherms and pore size distributions of (a) γ-Al_2O_3, (b) KF/γ-Al_2O_3, (c) La/γ-Al_2O_3, (d) KF-15La/γ-Al_2O_3, (e) KF-20La/γ-Al_2O_3, (f) KF-25La/γ-Al_2O_3, (g) KF-30La/γ-Al_2O_3, (h) KF-35La/γ-Al_2O_3.

Table 1. Specific surface area, pore volume and pore diameter of the different catalysts.

samples	S_{BET} ($m^2 g^{-1}$)	V_P ($cm^3 g^{-1}$)	D_P (nm)	amount of basic sites (mmol g^{-1})
γ-Al_2O_3	134.1	0.69	16.83	0.16
KF/γ-Al_2O_3	98.21	0.59	16.88	0.30
La/γ-Al_2O_3	86.12	0.49	16.88	0.24
KF-15La/γ-Al_2O_3	62.94	0.38	16.92	0.35
KF-20La/γ-Al_2O_3	54.86	0.28	22.58	0.41
KF-25La/γ-Al_2O_3	50.44	0.35	16.91	0.37
KF-30La/γ-Al_2O_3	41.82	0.23	22.56	0.43
KF-35La/γ-Al_2O_3	37.32	0.29	22.53	0.46

adsorption–desorption isotherms with an H_3 hysteresis loop, which is a typical feature of mesoporous materials. This indicates that the catalyst exhibited an irregular slit and crack structure, which is consistent with the structure of the γ-Al_2O_3 support, suggesting that the modification had no effect on the original structure of the catalyst.

After loading the γ-Al_2O_3 with KF and La_2O_3, the initial relative pressure of the hysteresis loops increased from 0.8 to 0.85 (figure 8d–h), and the relative pressure of the capillary condensation in the pores of the catalyst increased. In addition, with an increase in the La loading content, the distance between the adsorption and desorption branches of the catalyst decreased, thus weakening the capillary condensation phenomenon. This indicates that the number of small pores in the catalyst reduced, whereas the numbers of larger-diameter mesopores increased. Because a long-chain hydroxy ester was used as the raw material, the fine pores prevented the entry of the raw material into the pores of the catalyst. However, the small-diameter pores of the catalyst increased diffusion by resisting the entry of raw materials and prolonging the retention time of reactants and products [70]. This facilitated a cracking reaction and carbon deposition during the high-temperature reaction. Consequently, a large number of by-products were produced, thus reducing the selectivity of cyclopentadecanolide. These findings indicate that a reduction in the number of pores has a positive effect on the performance of the catalyst. This suggests that the production of large-diameter pores enhanced the diffusion rate of the hydroxy esters and the migration of molecules, which significantly affected the catalytic performance of the catalyst.

The pore size distribution diagram revealed that all the catalysts exhibited a wide pore size distribution with the main distribution range between 10 and 30 nm. With an increase in the La loading content, the numbers of large-diameter mesopores gradually increased. This could be attributed to the coverage of relatively small mesopores by KF and lanthanum oxide, and the formation of new materials, such as K_3AlF_6 and LaOF, which blocked the small mesopores.

Table 1 shows the specific surface area, pore volume and pore diameter of the various catalysts. For the single-load and double-load compounds, the specific surface area and pore volume of the catalyst
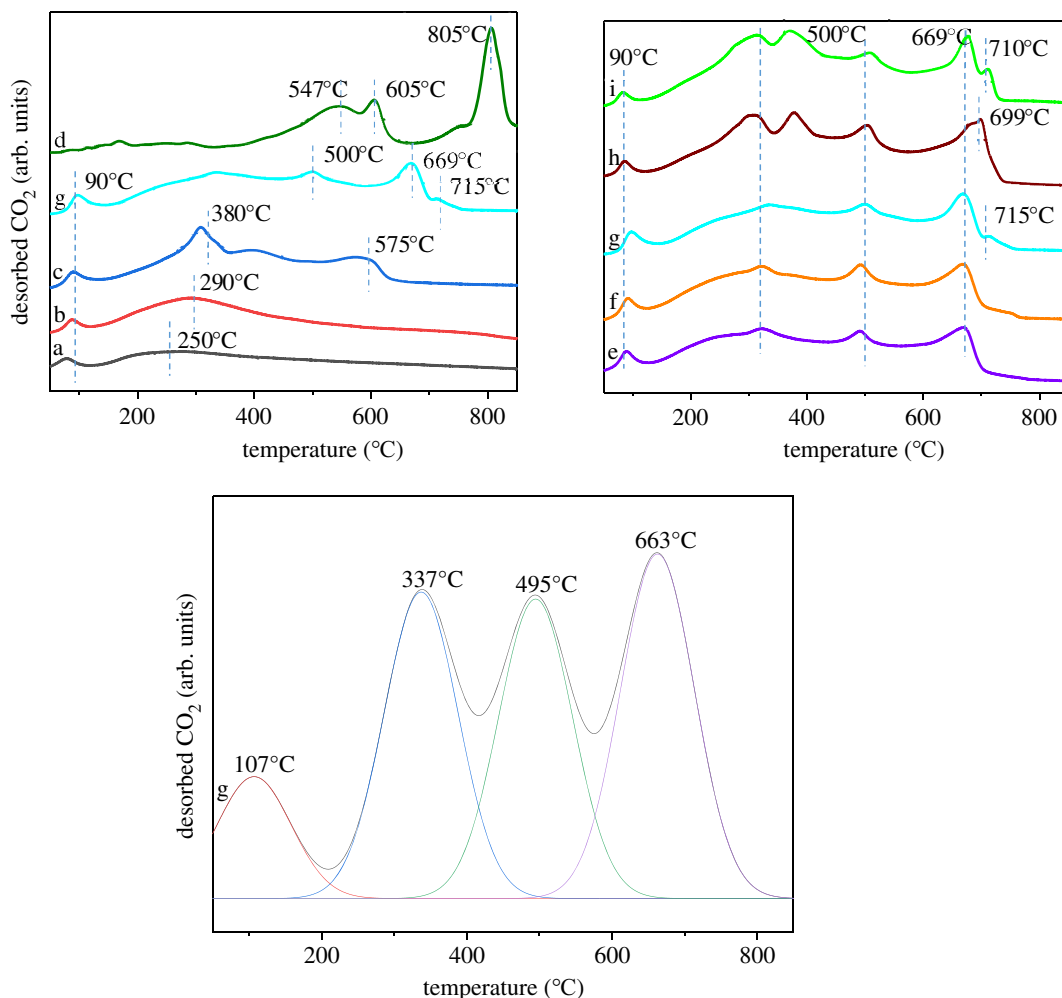
Figure 9. CO_2-TPD profiles of (a) γ-Al$_2$O$_3$, (b) La/γ-Al$_2$O$_3$, (c) KF/γ-Al$_2$O$_3$, (d) KF/La$_2$O$_3$, (e) KF-15La/γ-Al$_2$O$_3$, (f) KF-20La/γ-Al$_2$O$_3$, (g) KF-25La/γ-Al$_2$O$_3$, (h) KF-30La/γ-Al$_2$O$_3$, (i) KF-35La/γ-Al$_2$O$_3$.

decreased gradually with an increase in the La loading content. Nevertheless, the average pore diameter of the loaded catalyst was larger than that of pure γ-Al$_2$O$_3$, due to after the small pores were filled, the large pores dominate. The KF-25La/γ-Al$_2$O$_3$ catalyst exhibited a relatively large pore volume and the smallest average pore size. Owing to the full coverage of La$_2$O$_3$, the catalyst exhibited a better protective effect on the medium pore, which could be attributed to the fact that the small pore was filled and the high dispersion of KF on the surface of the catalyst. This was consistent with the XRD results. This shows that the specific surface area and pore size distribution have a huge influence on the catalytic performance of KF-La/γ-Al$_2$O$_3$.

3.1.5. Basicity of the catalyst

The strength of the basic sites of the catalysts was investigated using CO_2-TPD to understand the adsorption and desorption characteristics of CO_2 on the basic sites of the catalysts. The CO_2 desorption profiles are shown in figure 9.

The strength of basic is one of the most important indicators of solid base. With an increase in the interaction between the catalyst surface and CO_2, the CO_2 desorption temperature increased. Table 1 shows the CO_2 desorption content. A desorption peak was observed at approximately 90°C, which could be attributed to the desorption of CO_2 adsorbed in the γ-Al$_2$O$_3$ channel. As shown in figure 9d, no peak was observed at 90°C, which could be attributed to the extremely small specific surface area of KF/La$_2$O$_3$, lack of pore structure and weak physical adsorption of CO_2. A desorption peak was observed at 250°C, which was attributed to the weak basicity of Al$_2$O$_3$ (figure 9a), and an additional peak was

observed at 290°C, which could be attributed to the large radius of La, which increased the basicity of La_2O_3 compared with that of Al_2O_3. After the metal oxide was loaded with KF (figure 9c,d,g), the CO_2 desorption peaks shifted toward high temperature in comparison with that of the metal oxide catalyst (figure 9a,b). Because F^- ion has a higher electronegativity than O^{2-} ion, the negative charge of lattice oxygen was drawn toward F^- ion [67]. Thus, the KF-promoted metal oxide (Al_2O_3 or/and La_2O_3) contained more strong basic sites, compared with that of the corresponding metal oxide. Furthermore, CO_2 desorption peaks were observed at 500°C, 669°C and 715°C, indicating that the KF-25La/ γ-Al_2O_3 catalyst contained strong basic sites (figure 9g). This may be attributed to the formation of La_2O_3 and LaOF, and the fact that the atomic radius of La was larger than that of Al, thus facilitating the loss of electrons, which resulted in the generation of F^- anions. Consequently, the KF-25La/γ-Al_2O_3 catalyst exhibited a stronger Lewis base site and CO_2 interaction, thus increasing the desorption temperature of CO_2. KF/La_2O_3 exhibited the highest CO_2 desorption temperature, indicating that KF/La_2O_3 has a super base site; however, the specific surface area of KF/La_2O_3 was very small, thus limiting its catalytic effect.

A CO_2 desorption peak was observed at 669°C (figure 9e–i). With a decrease in La loading content below 25% (figure 9e,f), the CO_2 desorption temperature decreased. This could be attributed to the fact that the La load was small and did not completely cover the surface of γ-Al_2O_3, thus enabling the combination of Al with the excess KF to form a weak Lewis base site. However, with an increase in the La load beyond 25% (figure 9g–i), the desorption temperature of CO_2 increased. Consequently, a CO_2 desorption peak was observed in the pattern of KF-25La/γ-Al_2O_3 at 715°C. This could be attributed to the fact that the surface of γ-Al_2O_3 was fully covered with La_2O_3, and a large number of KF interacted with La_2O_3 to form strong Lewis base sites, which is consistent with the XRD and BET results. This indicates that the KF-25La/ γ-Al_2O_3 catalyst exhibited the strongest basicity and the best macrolactonization catalytic effect.

The desorption isotherm of KF-25La/γ-Al_2O_3 (figure 9g) can be divided into four small peaks. A weak alkali peak was observed at 107°C, which could be attributed to the medium-strong base peak at 337°C and 495°C, and a strong alkali peak was observed at 663°C. The two medium-strong alkali peaks could be attributed to the desorption of the CO_2 adsorbed on the outer surface of the catalyst at 337°C and the desorption peak at 495°C could be attributed to the adsorption of CO_2 inside the catalyst. The results of the CO_2-TPD characterization clearly show that we obtained a solid superbase with a maximum CO_2 desorption temperature of 715°C. This will be very favourable for the catalytic activity of our macrocyclization reaction.

Combining all the characterization results, we obtained solid superbases with a relatively uniform distribution of active sites, pore sizes ranging from 16.83 to 22.58 nm and specific surface areas ranging from 37.32 to 62.94 $m^2\,g^{-1}$.

3.2. Effects of the reaction conditions

Figure 10 shows the proposed mechanism of KF-La/γ-Al_2O_3-catalysed macrolactonization of methyl 15-hydroxypentadecanoate. Solid bases can accept protons or donate electrons when catalysing macrolactonization reactions. Assuming that the reaction took place on the surface of the catalyst, the first thing that occurs was that the alcohol and ester at both ends of the methyl 15-hydroxypentadecanoate were adsorbed on the active sites of the catalyst. Both the ester and alcohol then form intermediate on the active sites. The two ends of the intermediate react with each other to produce a cyclopentadecanolide molecule and a methanol molecule. This step was reversible, so it needed to be carried out under a vacuum, and the cyclopentadecanolide and methanol were continuously distilled out to ensure that the reaction was proceeding forward. After the reaction was completed, the active site of the catalyst catalysed other methyl 15-hydroxypentadecanoate reactions again.

3.2.1. Effect of the catalyst type on the cyclopentadecanolide yield

Cyclopentadecanolide was synthesized via a catalytic reaction of methyl 15-hydroxypentadecanoate using a series of catalysts. These catalysts include NaOH, γ-Al_2O_3, La/γ-Al_2O_3, KF/γ-Al_2O_3, KF/La_2O_3 and KF-La/ γ-Al_2O_3. The cyclopentadecanolide yield is shown in figure 11. The reaction was carried out using 0.5 g of the catalyst at a temperature and pressure of 190°C and 2 mbar, respectively, for 7 h. In the absence of a catalyst, the cyclopentadecanolide yield was 0%; however, the cyclopentadecanolide yield increased significantly after the addition of a catalyst. This indicates that the addition of catalysts significantly affects the macrolactonization of methyl 15-hydroxypentadecanoate.

When NaOH was used as a homogeneous catalyst to catalyse the macrolactonization of methyl 15-hydroxypentadecanoate, the cyclopentadecanolide yield was 41.29%. This could be attributed to the
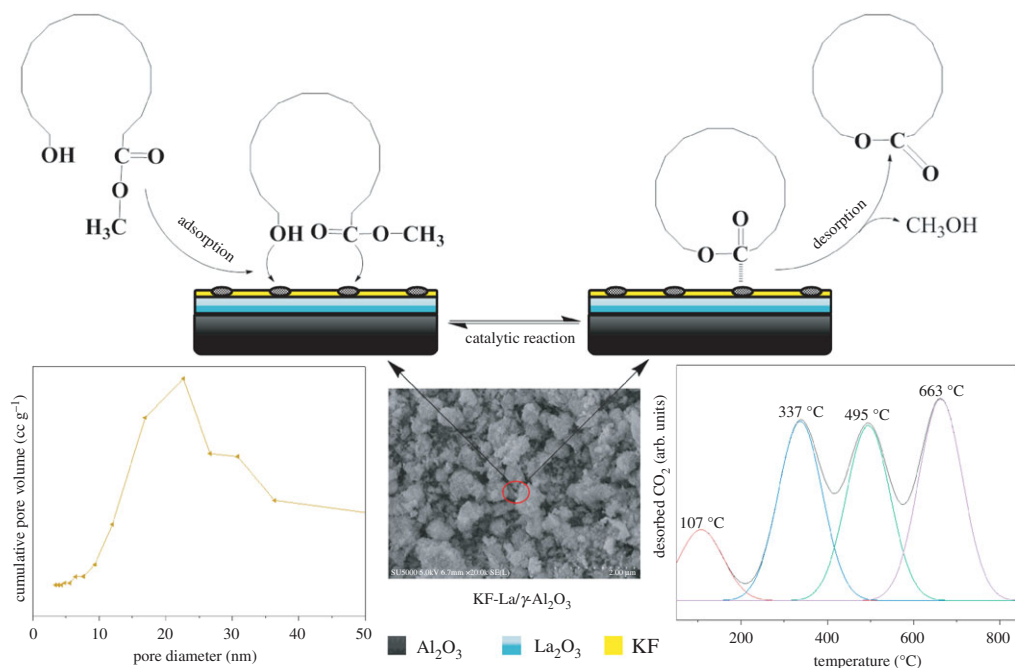
Figure 10. Proposed mechanism for macrolactonization of methyl 15-hydroxypentadecanoate with KF-La/γ-Al₂O₃ as catalyst.
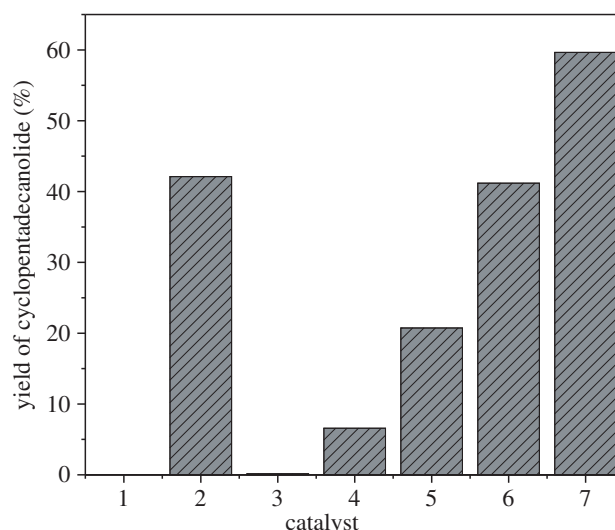

Figure 11. Comparison of the cyclopentadecanolide yields of the different catalysts. (1, no catalyst; 2, NaOH; 3, γ-Al₂O₃; 4, La/γ-Al₂O₃; 5, KF/γ-Al₂O₃; 6, KF/La₂O₃; 7, KF-La/γ-Al₂O₃).

strong corrosivity of NaOH and the fact that it is a strong base that facilitated the saponification of methyl 15-hydroxypentadecanoate under high temperature and vacuum condition. However, the reaction system was prone to explosive boiling and the temperature control was difficult. Consequently, a large amount of water was required to wash the substrate at the end of the reaction. Therefore, different solid base catalyst was used to catalyse the macrolactonization. The γ-Al₂O₃-supporter exhibited the lowest yield (0.14%), which could be attributed to the lack of alkali active centres in γ-Al₂O₃ owing to its large specific surface area. When γ-Al₂O₃ was loaded with La₂O₃, the cyclopentadecanolide yield increased to 6.45%, which could be attributed to the low basicity of La₂O₃, which provided base sites for γ-Al₂O₃. When γ-Al₂O₃ was loaded with KF, the basicity and base content of the catalyst improved; consequently, a cyclopentadecanolide yield of 20.34% was achieved, which was confirmed by CO₂-TPD.

The KF-La/γ-Al₂O₃ catalyst was obtained by sequentially loading La₂O₃ and KF on the surface of γ-Al₂O₃. Lanthanum oxide significantly affected the physical properties and catalytic activity of the catalyst. The La₂O₃ loaded on the surface of γ-Al₂O₃ interacted with KF to produce strong basic sites, while maintaining the large specific surface area and pore size of the catalyst. The addition of La
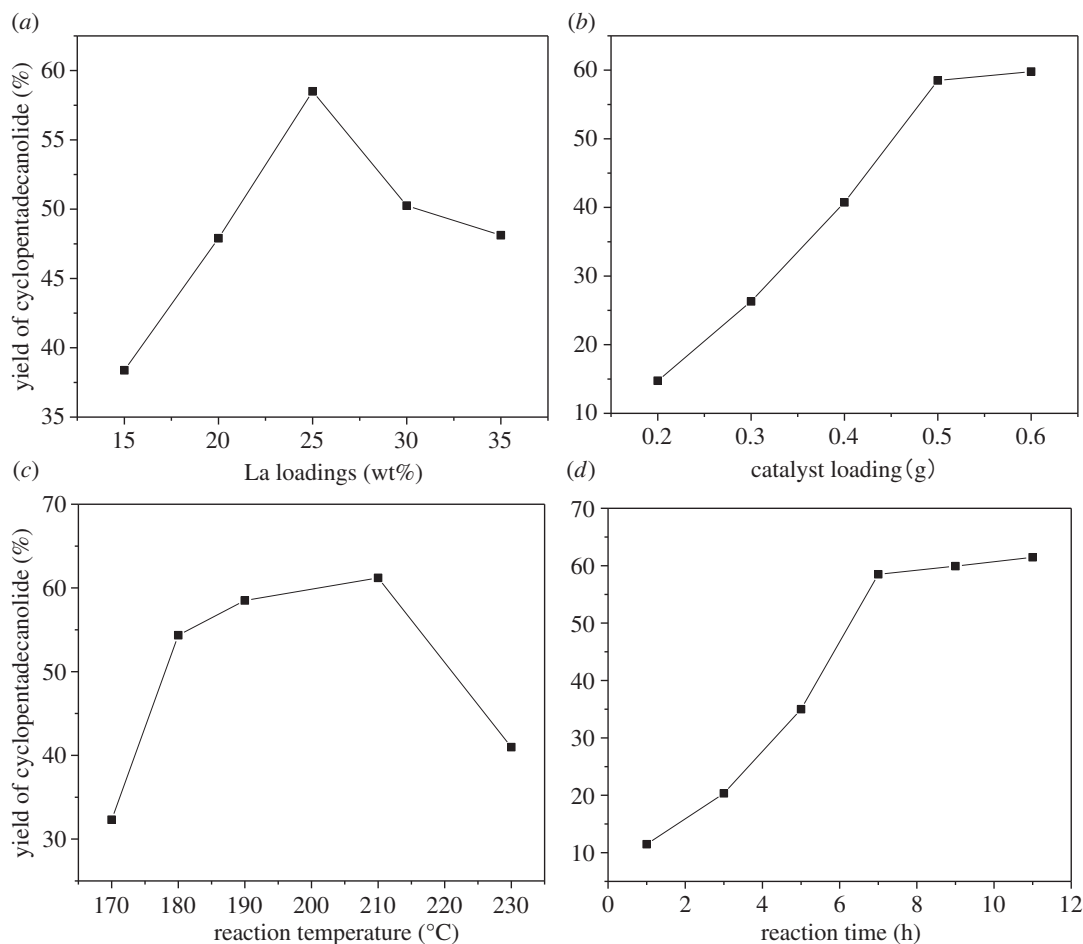
Figure 12. Effects of the reaction conditions: (*a*) La loading, (*b*) catalyst loading, (*c*) reaction temperature and (*d*) reaction time.

facilitated the formation of mesoporous solid strong base on the surface of γ-Al$_2$O$_3$. Using mesoporous γ-Al$_2$O$_3$ with a pore size of 16.8 nm as the catalyst support facilitated the entry of the long-chain hydroxy esters (i.e. methyl 15-hydroxypentadecanoate) into the inner surface of the catalyst to enable its contact with the active sites inside. These results were obtained using BET and CO$_2$-TPD. When the KF-(ω)La/γ-Al$_2$O$_3$ catalyst was used to catalyse the macrolactonization, a cyclopentadecanolide yield of 61.47% was achieved. However, when KF/La$_2$O$_3$ was used as the catalyst, the cyclopentadecanolide yield decreased, which could be attributed to the fact La$_2$O$_3$ has a small specific surface area regardless of its strong basicity, which restricted the reaction to the outer surface of metal oxides.

The cyclopentadecanolide yield of KF/La$_2$O$_3$ was lower than that of KF-(ω)La/γ-Al$_2$O$_3$ catalyst. These results indicate that the best catalyst for the synthesis of cyclopentadecanolide from methyl 15-hydroxypentadecanoate is a solid base catalyst with a large specific surface area, large pore size, strong basicity and a large amount of base active centre. Hence, KF-(ω)La/γ-Al$_2$O$_3$ was used as the catalyst for further investigations.

3.2.2. Effect of La loading on the cyclopentadecanolide yield

The effect of the La loading (15–35 wt%) of KF-ωLa/γ-Al$_2$O$_3$ on the macrolactonization of methyl 15-hydroxypentadecanoate was investigated, and the results are shown in figure 12*a*. The macrolactonization reaction was performed in a reduced pressure environment at 2 mbar. For this experiment, 0.5 g of the KF-(ω)La/γ-Al$_2$O$_3$ catalysts with various La loading content was used at 190°C for 7 h. With an increase in the La content from 15 to 25% w/w, the cyclopentadecanolide yield gradually increased. The low cyclopentadecanolide yield at low La loading content could be attributed to the fact that the La$_2$O$_3$ from the calcined La species did not completely cover the surface of the γ-Al$_2$O$_3$, resulting in fewer base sites and lower catalyst activity. With a further increase in the La content, the formed La$_2$O$_3$ layer interacted with KF to form more Lewis strong base sites. In addition, the excess La species filled the small pores and

prevented the cleavage of the long-chain methyl 15-hydroxypentadecanoate and cyclopentadecanolide due to the prolonged diffusion in the small pores. This indicates that the basic strength of the catalysts increased with an increase in the La loading from the TPD-CO_2 analysis. This indicates that a high basicity level facilitated this reaction. However, with a further increase in the La loading to 35 wt%, the cyclopentadecanolide yield decreased. With an increase in the La loading content, the coverage of the surface of the carrier by the La_2O_3 generated after calcination increased. Consequently, excess La_2O_3 agglomerated on the surface and pores of γ-Al_2O_3, resulting in a decrease in specific surface area of the supporter. These results are consistent with the XRD and BET results. These results indicate that the optimum La content that exhibit a moderate specific surface area, strongest basicity and highest cyclopentadecanolide yield, was 25% w/w.

3.2.3. Effect of catalyst loading on the cyclopentadecanolide yield

The effect of the KF-25La/γ-Al_2O_3 content on the macrolactonization of methyl 15-hydroxypentadecanoate was examined, and the results are shown in figure 12b. The catalyst content was varied between 0.2 and 0.6 g, while the other parameters, including pressure, catalyst loading and temperature were kept at 2 mbar, 0.5 g and 190°C, respectively. In the absence of a catalyst, no cyclopentadecanolide was formed; however, cyclopentadecanolide was produced after the addition of a catalyst. This indicates that the addition of a catalyst reduced the activation energy of the reaction and accelerated the macrolactonization rate. In addition, we found that the catalyst content affected the cyclopentadecanolide yield. With an increase in the catalyst loading from 0.2 to 0.6 g, the cyclopentadecanolide yield increased from 14.74 to 59.79%. An insufficient catalyst content resulted in incomplete macrolactonization. With an increase in the catalyst content, the cyclopentadecanolide yield increased. With an increase in the KF-25La/γ-Al_2O_3 content beyond 0.5 g, the yield increased gradually, indicating that the optimum catalyst content is 0.5 g.

3.2.4. Effect of temperature on the cyclopentadecanolide yield

Temperature is an important factor that affects macrolactonization. Therefore, the effect of the reaction temperature on the cyclopentadecanolide yield using KF-25La/γ-Al_2O_3 catalyst was investigated by varying the temperature from 170°C to 230°C, while other factors were kept constant, and the results are shown in figure 12c. With an increase in the temperature from 170°C to 210°C, the cyclopentadecanolide yield increased from 32.31% to 61.2%. However, the produced cyclopentadecanolide could not be extracted from the reaction system in time because the evaporation of glycerol decreases at a lower reaction temperature, thus increasing the resistance of the reaction equilibrium towards the direction of the product. Consequently, the cyclopentadecanolide yield decreased.

It was well known that an increase in the reaction temperature improves the reaction rate, and increases the evaporation of glycerine in the reaction system, thus enabling the acceleration of the reflux rate, the timely separation of the product and the shift in the reaction equilibrium toward the product. With an increase in temperature, the molecular motion increased, thus increasing the probability of collision between the hydroxyl groups and methoxy groups at the head and tail of methyl 15-hydroxypentadecanoate. Therefore, with an increase in the reaction temperature, the cyclopentadecanolide yield increased. However, with a further increase in the temperature to 230°C, the cyclopentadecanolide yield decreased. This could be attributed to the fact that extremely high temperatures trigger the saponification and carbonization of raw materials. In addition, excessive temperature affects the physical appearance of cyclopentadecanolide: for example, cyclopentadecanolide turns yellow. These results indicate that the optimum energy-saving temperature for the synthesis of good-quality cyclopentadecanolide is 190°C.

3.2.5. Effect of the reaction time on the cyclopentadecanolide yield

The effect of the reaction time on the cyclopentadecanolide yield was investigated, and the result is shown in figure 12d. The reaction time was varied between 1 and 11 h, while other reaction parameters were kept constant. The change in the cyclopentadecanolide yield with a change in the reaction time is shown in figure 12d. With an increase in the reaction time, the cyclopentadecanolide yield increased from 11.48 to 61.47%. With an increase in the reaction time from 1 to 7 h, the yield increased rapidly owing to the relatively high concentration of raw materials. In addition, the product was removed from the reaction system in time and the reaction equilibrium moved forward, thus increasing the yield rapidly. However, with a further increase in the reaction time beyond 7 h, the reaction rate decreased. As the reaction time increased, the concentration of raw materials decreased.
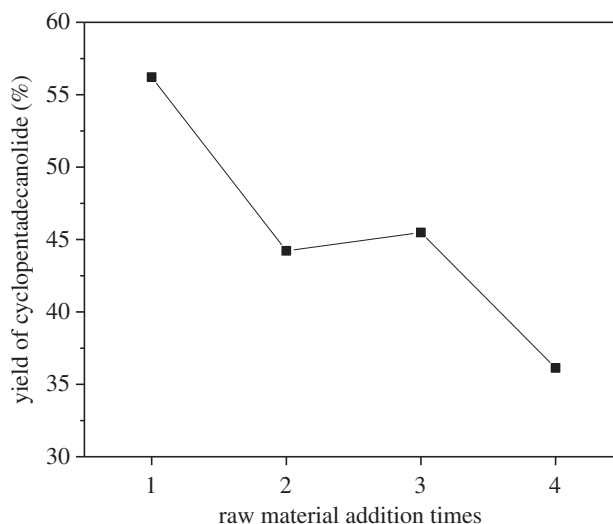
Figure 13. Continuous treatment of KF-La/γ-Al$_2$O$_3$.

Consequently, the cyclopentadecanolide that was not taken out in time was retained in the system, thus increasing the resistance of the reaction equilibrium to a positive movement. In addition, the reaction system was easily carbonized under long-term high temperature conditions, and a large number of by-products generated in the system covered the active sites of the catalyst and reduced the catalytic activity of the catalyst. These results indicate that the optimum reaction time to achieve an energy-saving macrolactonization of methyl 15-hydroxypentadecanoate to cyclopentadecanolide is 7 h. The yield and content of cyclopentadecanolide obtained under this condition were 58.50% and 98.80%, respectively.

3.3 Reusability study of KF-25La/γ-Al$_2$O$_3$

Reusability is one of the main advantages of heterogeneous catalysts. Thus, KF-25La/γ-Al$_2$O$_3$ recycling was investigated with respect to macrolactonization reactions. After the reaction, the glycerol at the bottom of the reactor is distilled out, and the raw materials and fresh glycerol were added to react again. The cyclopentadecanolide yield obtained is shown in figure 13. The reaction yield decreased with the second and third addition of raw materials. After the fourth addition of raw materials, the total cyclopentadecanolide yield reduced to 36.13%, by which time the catalyst had turned brown in colour. This low yield may be due to the presence of a large amount of materials and by-products in the reaction system blocking the pores of the catalyst, as well as coking of the catalyst caused by high temperatures, which reduces the activity of the catalyst.

According to the study above, a solid strong base KF-La/γ-Al$_2$O$_3$ with a large pore size that was synthesized at a relatively low calcination temperature in this paper was facile and energy-conserved since the process of preparation. KF and La were sequentially loaded on γ-Al$_2$O$_3$ to achieve three main functions. Firstly, the lanthanum oxide covering the surface of γ-Al$_2$O$_3$ promoted the uniform dispersion of KF (SEM-EDX images). Secondly, KF reacted with La species to produce strong basic active sites (CO$_2$-TPD). Lastly, KF and La species filled the small pores to prevent the prolonged diffusion of the large-molecular weight methyl 15-hydroxypentadecanoate through the small pores and cracking (BET). The catalytic performance of various types of catalysts was investigated, and the results revealed that the KF-25La/γ-Al$_2$O$_3$ catalyst exhibited the highest catalytic activity for the macrolactonization of methyl 15-hydroxypentadecanoate.

4. Conclusion

In this study, a solid base catalyst with large pore size was obtained under relatively mild calcination conditions using γ-Al$_2$O$_3$ as a support, which was used to catalyse the macrolactonization of methyl 15-hydroxypentadecanoate. The use of solid bases as catalysts relative to liquid catalysts reduces the risk of saponification of the raw materials. The reaction rectification method is adopted to shorten the reaction

time (7 h). The whole reaction uses cheap and easily available glycerol as a solvent and an entrainer, and no other toxic and harmful reagents are used, which avoids subsequent treatment and does not pose a threat to the environment. The yield and content of cyclopentadecanolide obtained under 0.5 g KF-25La/γ-Al$_2$O$_3$, 190°C and 7 h were 58.50% and 98.80%, respectively. The macrolactonization was carried out at a higher concentration (0.33 mol l^{-1}), and the obtained cyclopentadecanolide was of high purity, and no purification of the product was required. The catalyst can be re-used many times without treatment. KF-La/γ-Al$_2$O$_3$ solid base catalyst improves the overall synthesis efficiency and economy of cyclopentadecanolide, which can be extended to the synthesis of other macrolides.

References

1. Driggers EM, Hale SP, Lee J, Terrett NK. 2008 The exploration of macrocycles for drug discovery—an underexploited structural class. *Nat. Rev. Drug Discov.* **7**, 608–624. (doi:10.1038/nrd2590)

2. Winssinger N, Barluenga S. 2007 Chemistry and biology of resorcylic acid lactones. *Chem. Commun.* **1**, 22–36. (doi:10.1002/chin.200715233)

3. Parenty A, Moreau X, Niel G, Campagne JM. 2013 Update 1 of: Macrolactonizations in the total synthesis of natural products. *Chem. Rev.* **113**, 1–35. (doi:10.1021/cr300129n)

4. Jelić D, Antolović R. 2016 From erythromycin to azithromycin and new potential ribosome-binding antimicrobials. *Antibiotics* **5**, 1–13. (doi:10.3390/antibiotics5030029)

5. Kopp F, Stratton CF, Akella LB, Tan DS. 2012 A diversity-oriented synthesis approach to macrocycles via oxidative ring expansion. *Nat. Chem. Biol.* **8**, 358–365. (doi:10.1038/nchembio.911)

6. Wright AE, Botelho JC, Guzmán E, Harmody D, Linley P, McCarthy PJ, Pitts TP, Pomponi SA, Reed JK. 2007 Neopeltolide, a macrolide from a lithistid sponge of the family Neopeltidae. *J. Nat. Prod.* **70**, 412–416. (doi:10.1021/np060597h)

7. Kirst HA. 2010 ChemInform Abstract: The spinosyn family of insecticides: realizing the potential of natural products research. *ChemInform* **41**, 101–111. (doi:10.1002/chin.201025213)

8. Api AM *et al.* 2012 A toxicological and dermatological assessment of aryl alkyl alcohol simple acid ester derivatives when used as fragrance ingredients. *Food Chem. Toxicol.* **50**, S269–S313. (doi:10.1016/j.fct.2012.02.091)

9. Dodson RE, Nishioka M, Standley LJ, Perovich LJ, Brody JG, Rudel RA. 2012 Endocrine disruptors and asthma-associated chemicals in consumer products. *Environ. Health Perspect.* **120**, 935–943. (doi:10.1289/ehp.1104052)

10. Lefebvre C, Kimpe LE, Metcalfe CD, Trudeau VL, Blais JM. 2017 Bioconcentration of polycyclic musks in fathead minnows caged in a wastewater effluent plume. *Environ. Pollut.* **231**, 1593–1600. (doi:10.1016/j.envpol.2017.09.062)

11. Gao Y, Li G, Qin Y, Ji Y, Mai B, An T. 2019 New theoretical insight into indirect photochemical transformation of fragrance nitro-musks: mechanisms, eco-toxicity and health effects. *Environ. Int.* **129**, 68–75. (doi:10.1016/j.envint.2019.05.020)

12. Cheng H, Wei J, Liang M, Dai S, Liu X, Ma L, Wang H, Lai F. 2021 Calcium glycerolate catalyst derived from eggshell waste for cyclopentadecanolide synthesis. *Front. Chem.* **9**, 1–12. (doi:10.3389/fchem.2021.770247)

13. Williams AS. 1999 The synthesis of macrocyclic musks. *Synthesis (Stuttg.)* **10**, 1707–1723. (doi:10.1055/s-1999-3581)

14. Kurihara T, Nakajima Y, Mitsunobu O. 1976 Synthesis of lactones and cycloalkanes: cyclization of ω-hydroxy acids and ethyl α-cyano-ω-hydroxycarboxylates. *Tetrahedron Lett.* **17**, 2455–2458. (doi:10.1016/0040-4039(76)90018-6)

15. Shiina I, Kubota M, Oshiumi H, Hashizume M. 2004 An effective use of benzoic anhydride and its derivatives for the synthesis of carboxylic esters and lactones: a powerful and convenient mixed anhydride method promoted by basic catalysts. *J. Org. Chem.* **69**, 1822–1830. (doi:10.1021/jo030367x)

16. Boden EP, Keck GE. 1985 Proton-transfer steps in Steglich esterification: a very practical new method for macrolactonization. *Chem. Informationsd.* **16**, 2394–2395. (doi:10.1002/chin.198543260)

17. Li Y, Yin X, Dai M. 2017 Catalytic macrolactonizations for natural product synthesis. *Nat. Prod. Rep.* **34**, 1185–1192. (doi:10.1039/c7np00038c)

18. Stang EM, White MC. 2011 On the macrocyclization of the erythromycin core: preorganization is not required. *Angew. Chemie – Int. Ed.* **50**, 2094–2097. (doi:10.1002/anie.201007309)

19. Tatsumi T, Sakashita H, Asano K. 1993 Selective macrolactonization using zeolite molecular sieves. *J. Chem. Soc. Chem. Commun.* **1203**, 1264–1265. (doi:10.1039/C39930001264)

20. Stang EM, Christina White M. 2009 Total synthesis and study of 6-deoxyerythronolide B by late-stage C-H oxidation. *Nat. Chem.* **1**, 547–551. (doi:10.1038/nchem.351)

21. Watanabe T, Mutoh Y, Saito S. 2017 Ruthenium-catalyzed cycloisomerization of 2-alkynylanilides: synthesis of 3-substituted indoles by 1,2-carbon migration. *J. Am. Chem. Soc.* **139**, 7749–7752. (doi:10.1021/jacs.7b04564)

22. Trost BM, Rhee YH. 1999 Ruthenium-catalyzed cycloisomerization – oxidation of homopropargyl alcohols. A new access to γ-butyrolactones. *J. Am. Chem. Soc.* **121**, 11 680–11 683. (doi:10.1021/ja992013m)

23. Wang Y, Zheng Z, Zhang L. 2014 Ruthenium-catalyzed oxidative transformations of terminal alkynes to ketenes by using tethered sulfoxides: access to β-lactams and cyclobutanones. *Angew. Chemie – Int. Ed.* **53**, 9572–9576. (doi:10.1002/anie.201403796)

24. Evano G, Wang J, Nitelet A. 2017 Metal-mediated C-O bond forming reactions in natural product synthesis. *Org. Chem. Front.* **4**, 2480–2499. (doi:10.1039/c7qo00671c)

25. Kim I, Roh SW, Lee DG, Lee C. 2014 Rhodium-catalyzed oxygenative [2 + 2] cycloaddition of terminal alkynes and imines for the synthesis of β-lactams. *Org. Lett.* **16**, 2482–2485. (doi:10.1021/ol500856z)

26. Harras M, Milius W, Aitken RA, Schobert R. 2017 Syntheses of combretastatins D-1, D-2, and D-4 via ring contraction by flash vacuum pyrolysis. *J. Org. Chem.* **82**, 579–587. (doi:10.1021/acs.joc.6b02586)

27. Odedra A, Datta S, Liu RS. 2007 Ruthenium-catalyzed cyclization of 2-alkyl-1-ethynylbenzenes via a 1,5-hydrogen shift of ruthenium-vinylidene intermediates. *J. Org. Chem.* **72**, 3289–3292. (doi:10.1021/jo062573l)

28. Wu X, Neumann H, Beller M. 2012 Synthesis of heterocycles via palladium-catalyzed carbonylations. *Chem. Rev.* **113**, 1–35. (doi:10.1021/cr300100s)

29. Bai Y, Davis DC, Dai M. 2017 Natural product synthesis via palladium-catalyzed carbonylation. *J. Org. Chem.* **82**, 2319–2328. (doi:10.1021/acs.joc.7b00009)

30. Lumbroso A, Abermil N, Breit B. 2012 Atom economic macrolactonization and lactonization via redox-neutral rhodium-catalyzed coupling of terminal alkynes with carboxylic acids. *Chem. Sci.* **3**, 789–793. (doi:10.1039/c2sc00812b)

31. Spreider PA, Haydl AM, Heinrich M, Breit B. 2016 Rhodium-catalyzed diastereoselective cyclization of allenyl-sulfonylcarbamates: a stereodivergent approach to 1,3-aminoalcohol derivatives. *Angew. Chemie – Int. Ed.* **55**, 15 569–15 573. (doi:10.1002/anie.201609366)

32. Lee K, Kim H, Hong J. 2012 N-heterocyclic carbene catalyzed oxidative macrolactonization: total synthesis of (+)-dactylolide. *Angew. Chemie – Int. Ed.* **51**, 5735–5738. (doi:10.1002/anie.201201653)

33. Mukaiyama T, Izumi J, Shiina I. 1997 New and efficient method for the preparation of medium-sized lactones from the corresponding ω-hydroxycarboxylic acids. *Chem. Lett.* **26**, 187–188. (doi:10.1246/cl.1997.187)

34. Shiina I. 2004 An effective method for the synthesis of carboxylic esters and lactones using substituted benzoic anhydrides with Lewis acid catalysts. *Tetrahedron* **60**, 1587–1599. (doi:10.1016/j.tet.2003.12.013)

35. Ookoshi T, Onaka M. 1998 Zeolite-catalyzed macrolactonization of ω-hydroxyalkanoic acids in a highly concentrated solution. *Tetrahedron Lett.* **39**, 293–296. (doi:10.1016/S0040-4039(97)10545-7)

36. De Léséleuc M, Collins SK. 2015 Direct macrolactonization of seco acids via hafnium(IV) catalysis. *ACS Catal.* **5**, 1462–1467. (doi:10.1021/acscatal.5b00082)

37. Lai F, Liu X, Li W, Shen F. 2010 Macrolactonization of methyl 15-hydroxypentadecanoate to cyclopentadecanolide over Mo-Fe/HZSM-5 catalyst. *React. Kinet. Mech. Catal.* **100**, 407–415. (doi:10.1007/s11144-010-0196-9)

38. De Léséleuc M, Collins SK. 2015 Direct macrolactonization of seco acids via hafnium(IV)

39. catalysis. *ACS Catal.* **5**, 1462–1467. (doi:10.1021/acscatal.5b00082)

39. Funatomi T, Wakasugi K, Misaki T, Tanabe Y. 2006 Pentafluorophenylammonium triflate (PFPAT): an efficient, practical, and cost-effective catalyst for esterification, thioesterification, transesterification, and macrolactone formation. *Green Chem.* **8**, 1022–1027. (doi:10.1039/b609181b)

40. Fu W, Wang L, Yang Z, Shen JS, Tang F, Zhang J, Cui X. 2020 Facile access to versatile aza-macrolides through iridium-catalysed cascade allyl-amination/macrolactonization. *Chem. Commun.* **56**, 960–963. (doi:10.1039/c9cc07372h)

41. Xie W, Han Y, Wang H. 2018 Magnetic Fe$_3$O$_4$/MCM-41 composite-supported sodium silicate as heterogeneous catalysts for biodiesel production. *Renew. Energy* **125**, 675–681. (doi:10.1016/j.renene.2018.03.010)

42. Marwaha A, Dhir A, Mahla SK, Mohapatra SK. 2018 An overview of solid base heterogeneous catalysts for biodiesel production. *Catal. Rev. – Sci. Eng.* **60**, 594–628. (doi:10.1080/01614940.2018.1494782)

43. Zheng H, Hong Y, Xu J, Xue B, Li YX. 2018 Transesterification of ethylene carbonate to dimethyl carbonate catalyzed by CeO$_2$ materials with various morphologies. *Catal. Commun.* **106**, 6–10. (doi:10.1016/j.catcom.2017.12.007)

44. Xie W, Zhao L. 2013 Production of biodiesel by transesterification of soybean oil using calcium supported tin oxides as heterogeneous catalysts. *Energy Convers. Manag.* **76**, 55–62. (doi:10.1016/j.enconman.2013.07.027)

45. Xie W, Wan F. 2018 Basic ionic liquid functionalized magnetically responsive Fe$_3$O$_4$@HKUST-1 composites used for biodiesel production. *Fuel* **220**, 248–256. (doi:10.1016/j.fuel.2018.02.014)

46. Ivan-Tan CT, Islam A, Yunus R, Taufiq-Yap YH. 2017 Screening of solid base catalysts on palm oil based biolubricant synthesis. *J. Clean. Prod.* **148**, 441–451. (doi:10.1016/j.jclepro.2017.02.027)

47. Cong WJ, Wang YT, Li H, Fang Z, Sun J, Liu HT, Liu JT, Tang S, Xu L. 2020 Direct production of biodiesel from waste oils with a strong solid base from alkalized industrial clay ash. *Appl. Energy* **264**, 114735. (doi:10.1016/j.apenergy.2020.114735)

48. Yu X, Chen X, Meng W, Zhu M. 2021 Research progress on supported solid superbase and its catalytic application. *Chem. Pap.* **75**, 4445–4463. (doi:10.1007/s11696-021-01669-w)

49. Xie J, Chen L, Au CT, Yin SF. 2015 Synthesis of KOH/SnO$_2$ solid superbases for catalytic Knoevenagel condensation. *Catal. Commun.* **66**, 30–33. (doi:10.1016/j.catcom.2015.03.008)

50. Unnikrishnan P, Srinivas D. 2012 Calcined, rare earth modified hydrotalcite as a solid, reusable catalyst for dimethyl carbonate synthesis. *Ind. Eng. Chem. Res.* **51**, 6356–6363. (doi:10.1021/ie300678p)

51. Sun C, Qiu F, Yang D, Ye B. 2014 Preparation of biodiesel from soybean oil catalyzed by Al-Ca hydrotalcite loaded with K$_2$CO$_3$ as heterogeneous solid base catalyst. *Fuel Process. Technol.* **126**, 383–391. (doi:10.1016/j.fuproc.2014.05.021)

52. Gao L, Xu B, Xiao G, Lv J. 2008 Transesterification of palm oil with methanol to biodiesel over a KF/hydrotalcite solid catalyst. *Energy Fuels* **22**, 3531–3535. (doi:10.1021/ef800340w)

53. Sandesh S, Shanbhag G V, Halgeri AB. 2013 Transesterification of glycerol to glycerol carbonate using KF/Al$_2$O$_3$ catalyst: the role of support and basicity. *Catal. Lett.* **143**, 1226–1234. (doi:10.1007/s10562-013-1043-1)

54. Wang L, Ma Y, Wang Y, Liu S, Deng Y. 2011 Efficient synthesis of glycerol carbonate from glycerol and urea with lanthanum oxide as a solid base catalyst. *Catal. Commun.* **12**, 1458–1462. (doi:10.1016/j.catcom.2011.05.027)

55. Song R, Tong D, Tang J, Hu C. 2011 Effect of composition on the structure and catalytic properties of KF/Mg-La solid base catalysts for biodiesel synthesis via transesterification of cottonseed oil. *Energy Fuels* **25**, 2679–2686. (doi:10.1021/ef200378j)

56. Niu X, Xing C, Jiang W, Dong Y, Yuan F, Zhu Y. 2013 Activity and stability of solid base KF/La$_2$O$_3$ catalysts for transesterification of tributyrin with methanol. *React. Kinet. Mech. Catal.* **109**, 167–179. (doi:10.1007/s11144-013-0543-8)

57. Liu N, Wu Z, Li M, Li S, Luo Z, Li Y, Pan L, Liu Y. 2016 Low-temperature preparation of mesoporous solid superbases by using multifunction of a La$_2$O$_3$ interlayer. *ChemCatChem* **12**, 3–8. (doi:10.1002/cctc.201601246)

58. Hu F, Wang Y, Lai X, Wu Y, Du F, Wang C. 2015 Facile synthesis of mesoporous Si-containing γ-Al$_2$O$_3$ nanofiber with enhanced thermal stability. *Chem. Res. Chinese Univ.* **31**, 156–159. (doi:10.1007/s40242-015-4322-0)

59. Čejka J. 2003 Organized mesoporous alumina: synthesis, structure and potential in catalysis. *Appl. Catal. A Gen.* **254**, 327–338. (doi:10.1016/S0926-860X(03)00478-2)

60. Fedorov A V, Gulyaeva YK. 2019 Strength statistics for porous alumina. *Powder Technol.* **343**, 783–791. (doi:10.1016/j.powtec.2018.11.098)

61. Shahraki H, Entezari MH, Goharshadi EK. 2015 Sono-synthesis of biodiesel from soybean oil by KF/γ-Al$_2$O$_3$ as a nano-solid-base catalyst. *Ultrason. Sonochem.* **23**, 266–274. (doi:10.1016/j.ultsonch.2014.09.010)

62. Xie W, Peng H, Chen L. 2006 Transesterification of soybean oil catalyzed by potassium loaded on alumina as a solid-base catalyst. *Appl. Catal. A Gen.* **300**, 67–74. (doi:10.1016/j.apcata.2005.10.048)

63. Garbarino G, Wang C, Cavattoni T, Finocchio E, Riani P, Flytzani-Stephanopoulos M, Busca G. 2019 A study of Ni/La-Al$_2$O$_3$ catalysts: a competitive system for CO$_2$ methanation. *Appl. Catal. B Environ.* **248**, 286–297. (doi:10.1016/j.apcatb.2018.12.063)

64. Béguin B, Garbowski E, Primet M. 1991 Stabilization of alumina by addition of lanthanum. *Appl. Catal.* **75**, 119–132. (doi:10.1016/S0166-9834(00)83128-0)

65. Dong AH, Wang K, Zhu SZ, Yang GB, Wang XT. 2017 Facile preparation of PtSn-La/Al$_2$O$_3$ catalyst with large pore size and its improved catalytic performance for isobutane dehydrogenation. *Fuel Process. Technol.* **158**, 218–225. (doi:10.1016/j.fuproc.2017.01.004)

66. Rana MS, Ancheyta J, Maity SK, Rayo P. 2005 Characteristics of Maya crude hydrodemetallization and hydrodesulfurization catalysts. *Catal. Today* **104**, 86–93. (doi:10.1016/j.cattod.2005.03.059)

67. Liu N, Wu Z, Li M, Li S, Li Y, Yu R, Pan L, Liu Y. 2017 A novel strategy for constructing mesoporous solid superbase catalysts: bimetallic Al-La oxides supported on SBA-15 modified with KF. *Catal. Sci. Technol.* **7**, 725–733. (doi:10.1039/c6cy02334g)

68. Jiang W, Niu X, Yuan F, Zhu Y, Fu H. 2014 Preparation of KF-La$_2$O$_2$CO$_3$ solid base catalysts and their excellent catalytic activities for transesterification of tributyrin with methanol. *Catal. Sci. Technol.* **4**, 2957–2968. (doi:10.1039/c4cy00167b)

69. Sun LB, Liu XQ, Zhou HC. 2015 Design and fabrication of mesoporous heterogeneous basic catalysts. *Chem. Soc. Rev.* **44**, 5092–5147. (doi:10.1039/c5cs00090d)

70. Ma L, Jia I, Guo X, Xiang L. 2014 High performance of Pd catalysts on bimodal mesopore for the silica catalytic oxidation of toluene. *Chinese J. Catal.* **35**, 108–119. (doi:10.1016/S1872)

71. Cheng H, Yu C, Wang H, Liu X, Ma L, Lai F. 2022 Macrolactonization of methyl 15-hydroxypentadecanoate to cyclopentadecanolide using KF-La/γ-Al$_2$O$_3$ catalyst. Figshare. (doi:10.6084/m9.figshare.c.6182406)